CONTRIBUTIONS TO BLAST WAVE AND FRACTURE THEORIES

By

SABODH K. GARG

A DISSERTATION PRESENTED TO THE GRADUATE COUNCIL OF
THE UNIVERSITY OF FLORIDA
IN PARTIAL FULFILLMENT OF THE REQUIREMENTS FOR THE
DEGREE OF DOCTOR OF PHILOSOPHY

UNIVERSITY OF FLORIDA

June, 1965

PREFACE

The present investigations form a part of a study dealing with the response of a thin spherical shell subject to an internal explosion, being carried on in the Department of Engineering Science and Mechanics at the University of Florida under a research contract from the U.S. Army Biological Laboratories, Fort Detrick, Maryland. The general problem is exceedingly complex and requires effort in such diverse fields as detonation chemistry, blast waves, stress waves in solid media, fracture, vibration theory and reflection phenomena. It has been possible to deal here only with a selected number of topics.

Chapter I and II deal with the calculation of pressure behind the shock front in a blast wave generated by a finite source. Theoretical calculations are supplemented by experimental data obtained at the University of Florida. In Chapter III, the nature of fracture under impulsive loading is examined. An empirical criterion for number of fragments based upon the experimental data

obtained at Fort Detrick is proposed. Finally, in Chapter IV, pressure calculations are related to the fracture study through the introduction of the concept of fracture times.

It is always hard for a graduate student to list all of the sources of his intellectual inspiration. Here, only some more pressing obligations can be met. During two years of work on this problem, the author received much valuable help in exploring new ideas from Dr. J. Siekmann, chairman of the supervisory committee. Mr. D. W. Falconer of Army Biological Laboratories was responsible for making available experimental data on fracture. Mr. D. Mitchell was invaluable in conducting the experimental work here. Thanks are also due to Dr. W. A. Nash, Chairman of the Department of Engineering Science and Mechanics for providing financial assistance.

TABLE OF CONTENTS

	Page
PREFACE	ii
LIST OF TABLES	vi
LIST OF FIGURES	vii
NOMENCLATURE	viii
ABSTRACT	x
CHAPTER	
I. APPROXIMATE SOLUTION OF THE PROPAGATION OF AN AXISYMMETRIC BLAST WAVE GENERATED BY A FINITE SPHERICAL CHARGE	1
1. Introduction	1
2. Equations of Motion and Boundary Conditions	4
3. Numerical Calculations for Spherical Blast Waves	23
4. Numerical Calculations for Axisymmetrical Point-Source-Finite-Energy Blast Wave	31
5. Conclusions	38
II. SOME EXPERIMENTAL RESULTS FOR BLAST WAVES ORIGINATING FROM A FINITE SOURCE	41
1. Introduction	41
2. Equipment and Procedure	42

TABLE OF CONTENTS (Continued)

		Page
	3. Experimental Results	46
	4. Expansion of Explosion Products	50
	5. Pressure Calculations	52
III.	ON FRACTURE OF A THIN SPHERICAL SHELL UNDER BLAST LOADING	54
	1. Introduction	54
	2. Fracture Criteria	55
	3. On Shell Fragmentation	58
	4. Experimental Program	61
	5. Some Dimensional Considerations	69
	6. Conclusions	71
IV.	ON THE CALCULATION OF FRACTURE TIME FOR THIN SPHERICAL SHELLS SUBJECT TO INTERNAL BLAST LOADING	72
	1. Introduction	72
	2. Preliminary Considerations	73
	3. Thin Shell Simplifications	74
	4. Experimental Results	75
V.	CONCLUSIONS	78
LIST OF REFERENCES		79
BIOGRAPHICAL SKETCH		82

LIST OF TABLES

Table		Page
1.	Spherical Symmetric Point Source Explosion: Comparison of Taylor's [6] Results with the Author's	26
2.	B, f and g as Functions of θ	35
3.	Numerical Results for Axisymmetrical Case [$\gamma = \gamma_o = 1.2$, $n = 1.5$] . . .	36
4.	Numerical Results for Axisymmetrical Case [$\gamma = \gamma_o = 1.4$, $n = 1.5$] . . .	39
5.	Experimental Results for Finite Energy Blast Waves	47
6.	Experimental Results on Fracture	66
7.	Additional Experimental Results on Fracture	68
8.	Calculation of Fracture Times	77

LIST OF FIGURES

Figure		Page
1.	Geometry of the Explosion	5
2.	Flow behind the Main Shock	22
3.	Plot of f Versus η	27
4.	Plot of h Versus η	28
5.	Plot of k Versus η	29
6.	Sketch of Axisymmetric Shock Surface . . .	34
7.	Test Stand	43
8.	A Typical Firing Sequence for 0.6 gm PBRDX Charge	45
9.	Variation of Shock Head Velocity with Shock Radius	49
10.	Propagation of Stress-Waves in Media . . .	59
11.	Combination of Shell, Detonator and Charge Prior to Assembly	62
12.	Fracture of 1 11/16 Inch Diameter Plastic Sphere. Charge Weight: 1.3 grams. Frame Rate: 500,000 Frames/Second . . .	64

NOMENCLATURE

a	Radius of explosive charge
A	Dimensional Constant
$B(\theta)$	Constant for specified θ
c_o	Velocity of sound in air
E	Energy of explosion
f, g, h, k	Nondimensional flow variables
F, G, H, K	Dimensional flow variables
I	Impulse
ℓ, m, n	Nondimensional exponents
M	Mass
N	Number of fragments
p	Pressure
P	Dynamic pressure
r, θ	Spherical Polar coordinates
R	Shock-radius
t	Time
v_r, u	Velocity in radial direction
v_θ, v	Velocity in meridional direction
U	Velocity of shock head

NOMENCLATURE (Continued)

V	Particle velocity
V_{cr}	Critical velocity of straining
γ	Ratio of specific heats
η	Similarity variable
λ^*	= (N/V)
λ	Angle between shock radius and normal to shock head

Abstract of Dissertation Presented to the Graduate Council
in Partial Fulfillment of the Requirements for the
Degree of Doctor of Philosophy

CONTRIBUTIONS TO BLAST WAVE
AND FRACTURE THEORIES

By

Sabodh K. Garg

June, 1965

Chairman: Dr. Julius Siekmann
Major Department: Engineering Science and Mechanics

Proceeding from general mathematical and physical considerations, a group of similarity transformations has been obtained for the case of axisymmetric flow when the Euler equations are given in spherical coordinates. Previous similarity solutions due to G. I. Taylor are shown to be special cases of these transformations. It is also shown that while these transformations cannot be applied consistently to obtain an exact solution for the case of a blast wave generated by a finite source, they may be used to find an approximate solution. Numerical results are presented for the spherical blast

wave resulting from a finite source; and an axisymmetric blast wave generated by a point-source-finite-energy explosion.

A method employing a multi-spark camera device for obtaining the Schlieren record is presented. Two examples for very short time following the explosion are given. For these cases, the calculation of flow variables in the contact front is discussed.

Rinehart and Pearson's criterion for rupture of cylindrical shells is extended to spherical shells. An experimental program on polystyrene plastic shells of different sizes is reported. The dominant fracture pattern observed was brittle. Also, critical velocity of straining (V_{cr}) was found to be directly proportional to the cube of the diameter of the shell. On the basis of dimensional considerations, it is shown that shell wall thickness has no effect on the number of fragments. Finally, the effect of material properties on the critical velocity of straining and the number of fragments is investigated.

Fracture time is defined as the period that must elapse between the impingement of the blast wave on the surface of the shell and the rupture of the shell. A

formula for calculation of fracture time is obtained by equating the impulse imparted to the final momentum of the shell. A simplified form of the formula is applied for calculation of fracture times for thin shells. It is observed that fracture time is dependent upon dynamic pressure.

CHAPTER I

APPROXIMATE SOLUTION OF THE PROPAGATION OF AN AXISYMMETRIC BLAST WAVE GENERATED BY A FINITE SPHERICAL CHARGE

1. Introduction

An explosion generally consists of a sudden release of a finite amount of energy from a small quantity of solid, liquid or gas; and an explosive is any such solid, liquid or gas. Detonation refers to the propagation of shock wave in combustible media, whereas blast refers to its propagation in compressible noncombustible media.

Theoretical and experimental investigations have been directed on the one hand to the calculation of the equation of state of the explosion products [1, 2], and on the other hand to the propagation of shock waves in various media. Sir G. I. Taylor [3] discussed the dynamics of detonation fronts in solid explosives. Recently considerable interest has been generated in detonation in gases due to its applications in rocketry. A survey of

progress in this direction is contained in A. Oppenheim, et al. [4]. In this paper, while no study of detonation as such is undertaken, it is demonstrated, that Taylor's solution [3] forms a special case of the transformation set derived.

A detailed review of the literature concerning blast waves in gases was given by I. I. Glass [5]. In the following, only the work pertinent to the present investigation will be discussed. G. I. Taylor [6] solved the problem of a spherical blast wave arising from an intense point source explosion in air and predicted that pressure will be attenuated with distance as $1/R^3$, where R denotes the shock wave radius. While his results generally agreed with observed experimental phenomena for moderate values of R, agreement was not as good for small and large values of R. The same problem has also been solved analytically by L. I. Sedov [7], J. von Neumann [8], J. L. Taylor [9] and R. Latter [10]. J. A. McFadden [11] tried to provide solutions for short times after the detonation. His method is applicable, however, to a distance of only five per cent of the explosive radius. H. L. Brode [12] has attempted to provide numerical solutions of the complete equations for

spherical blast waves. Brode predicts that pressure will attenuate at a rate proportional to $1/R$ for small values of R, and as $1/R^3$ for moderate values of R, when the explosion products have absorbed ambient gases approximately ten times their mass. In the intermediate range, pressure decays as $1/R^{2n}$, where $0.5 < n < 1.5$. These results for a particular charge of T.N.T. agree reasonably well with those of F. J. Berry et al. [13].

In the present work, general similarity transformations are derived for axisymmetric fluid motion employing Euler's equations in spherical coordinates, and reducing them together with the continuity equation to a system of four ordinary differential equations. It is shown that G. I. Taylor's solutions [3, 6, 14] are special cases of these. The applicability of the Rankine-Hugoniot conditions at the shock front has been examined. It is demonstrated that it is possible to satisfy them only under the strong shock assumptions. Numerical examples are provided for the cases of (i) spherical blast waves originating from a finite charge and (ii) axisymmetrical blast wave generated by a finite-energy-point-source explosion.

2. Equations of Motion and Boundary Conditions

The blast wave is assumed to originate from a sphere filled with explosive and encircled by a diaphragm around its periphery in the equatorial plane (see Figure 1). It is suggested by the geometry that one must consider the variation of flow variables not only in the radial direction, but also in the θ, or meridional direction. Assuming that the products of explosion can be approximated by a perfect, adiabatic, inviscid gas, the equations of continuity, momentum and energy may be expressed in spherical coordinates as follows:

Equation of Continuity

$$\frac{\partial \rho}{\partial t} + \left[\frac{2}{r} v_r \rho + \frac{\partial v_r}{\partial r} \rho + v_r \frac{\partial \rho}{\partial r} + \frac{v_\theta}{r} \cdot \frac{\partial \rho}{\partial \theta} + \frac{\rho}{r} \frac{\partial v_\theta}{\partial \theta} + \frac{\rho v_\theta}{r} \cot \theta \right] = 0 \quad (1)$$

Equations of Momentum

$$\frac{\partial v_r}{\partial t} + v_r \frac{\partial v_r}{\partial r} + \frac{v_\theta}{r} \frac{\partial v_r}{\partial \theta} - \frac{v_\theta^2}{r} = - \frac{1}{\rho} \frac{\partial p}{\partial r} \quad (2)$$

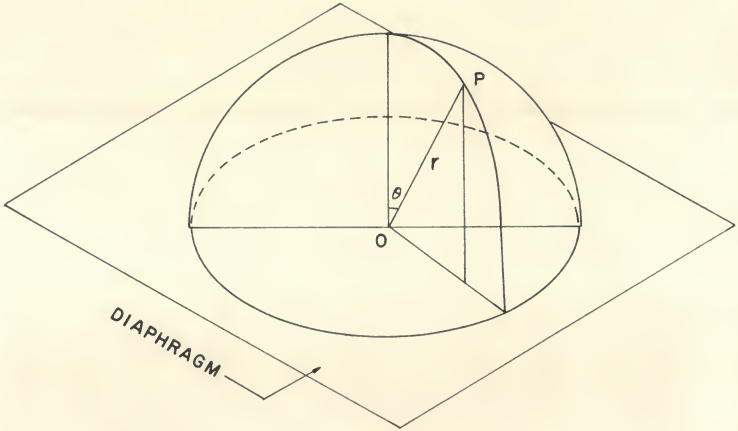

Figure 1: Geometry of the Explosion

$$\frac{\partial v_\theta}{\partial t} + v_r \frac{\partial v_\theta}{\partial r} + \frac{v_\theta}{r} \frac{\partial v_\theta}{\partial \theta} + \frac{v_r v_\theta}{r} = -\frac{1}{\rho r} \frac{\partial p}{\partial \theta} \qquad (3)$$

Equation of Reversible Adiabatic Change of State

$$\frac{\partial}{\partial t}\left(\frac{p}{\rho^\gamma}\right) + v_r \frac{\partial}{\partial r}\left(\frac{p}{\rho^\gamma}\right) + \frac{v_\theta}{r} \cdot \frac{\partial}{\partial \theta}\left(\frac{p}{\rho^\gamma}\right) = 0 \qquad (4)$$

where v_r denotes the velocity in the radial direction, v_θ the velocity in the meridional direction, p the pressure, ρ the density and γ the ratio of specific heats. In real gases, the specific heat of a gas may be approximated by a power series in temperature. It then becomes possible to calculate a mean specific heat for a particular temperature range from the relation (see Reference 15).

$$\bar{c}_v = \frac{1}{T_2 - T_1} \int_{T_1}^{T_2} c_v \, dT \quad , \quad \bar{c}_p = \frac{1}{T_2 - T_1} \int_{T_1}^{T_2} c_p \, dT$$

Using this relation, a mean value for γ over this temperature range can be determined

$$\bar{\gamma} = \bar{c}_p / \bar{c}_v$$

Thus, for air in the range of temperatures and pressures usually encountered in blasts from conventional explosives [13], $\bar{\gamma} = 1.2$ gives a fairly good approximation.

The equations (1-4) are to be solved with regard to a suitable set of initial and boundary conditions which will be specified later.

Since an analytical treatment of the set of nonlinear equations (1-4) presents mathematical difficulties beyond the present power of analysis one has to rely on numerical or similarity methods. A powerful technique is finding a group of transformations reducing the set of partial differential equations to a system of ordinary differential equations. In what follows, the transformations will be obtained for shock waves generated by an instantaneous release of a finite amount of energy from a finite source.

A first step in the process of seeking similarity transformations is the selection of a suitable similarity variable, which should preferably be dimensionless. Since the flow field has two characteristics lengths, i.e., the shockwave radius R (θ, t), and the radius locating any point of interest in the flow field, r, it would then seem reasonable to assume the following form of similarity variable:

$$\eta = \frac{r}{R(\theta,t)}$$

The next step is to seek from physical reasoning, forms suitable for the dependent variables. In the most general case the following transformations may be used:

$$V_r = U = \alpha^*(r,\theta,t)\,F(\eta),\quad V_\theta = V = \beta^*(r,\theta,t)G(\eta),$$

$$P/P_0 = \gamma^*(r,\theta,t)\,H(\eta),\quad \rho/\rho_0 = \delta^*(r,\theta,t)\,K(\eta).$$

α^*, β^*, γ^* and δ^* are functions of r, θ and t. The subscript o refers to the ambient atmosphere. However, this might be too general to be of much help in a specific problem. A particular subset of it which is useful in the present problem may be written as:

$$U = R^{-n_1} F(\eta),\quad V = R^{-n_2} G(\eta),$$

$$P/P_0 = R^{-m} H(\eta),\quad \rho/\rho_0 = R^{-\ell} K(\eta), \qquad (5)$$

where n_1, n_2, ℓ and m are positive or negative constants. As will be shown below, their choice is not completely arbitrary.

Substituting from (5) into the continuity equation (1), one obtains

$$-R^{-\ell}\frac{\partial R}{\partial t}\left[\eta K' + \ell K\right]\eta + R^{-(\ell+n_1)}\cdot$$
$$\left[\eta F'K + \eta FK' + 2KF\right] - \left[\frac{G\ell K}{R}\frac{\partial R}{\partial \theta} + \right.$$
$$\left.\frac{\eta K'G}{R}\frac{\partial R}{\partial \theta} + \frac{\eta G'K}{R}\frac{\partial R}{\partial \theta}\right]\cdot R^{-(\ell+n_2)}$$
$$+ KGR^{-(\ell+n_2)}\cot\theta = 0$$

where a prime denotes differentiation with respect to η. The equation can be made independent of R by putting

$$\frac{\partial R}{\partial t} = AR^{-n}, \quad A = \text{constant},$$
$$\frac{\partial R}{\partial \theta} = B(\theta)R \tag{6}$$

with

$$n = n_1 = n_2 \tag{7}$$

For the time being, nothing more will be said about the nature of A and B (θ). The problem of their evaluation will be treated later.

Another useful relation between ℓ, m and n is obtained by substituting from equations (5-7) into

the first equation of momentum (2). This yields:

$$-A\eta[nF+F'\eta]R^{-2n}+F'R^{-2n}\cdot$$
$$[F\eta-GB\eta]-nBR^{-2n}FG-R^{-2n}G^2$$
$$=\frac{c_o^2}{\gamma_o K}R^{l-m}H'\eta\ ,$$

where $c_o^2=\gamma_o P_o/\rho_o$ denotes the velocity of sound in the ambient atmosphere. To make this equation independent of R, the following is required

$$m=l+2n \tag{8}$$

No additional relation between l and n can be obtained by substitution in (3) and (4).

From (5-8), the general set of transformations reducing the partial differential equations of flow (1-4) for the flow field between the shock wave and the origin to ordinary ones may be written as follows:

$$u=R^{-n}F(\eta)\ ,\ v=R^{-n}G(\eta)\ ,$$
$$P/P_o=R^{-(l+2n)}H(\eta)\ ,\ \rho/\rho_o=R^{-l}K(\eta)\ ,$$
$$\partial R/\partial t=AR^{-n}\ ,\ \frac{\partial R}{\partial\theta}=B(\theta)R\ , \tag{9}$$

where l and n are arbitrary constants.

Set (9) allows a double-infinite manifold of transformations for selected values of ℓ and n. This point may further be illustrated by reference to the classical Taylor problem of spherical detonation and blast waves.

(i) Spherical detonation wave emerging from geometric center of the explosive: Assuming the detonation wave to be spherically symmetric, one has B = G = 0 and R = R(t). Further $\partial R/\partial t = dR/dt = A =$ constant. Then taking $n = \ell = 0$, equations (9) reduce to:

$$u = F(\eta), \quad p/p_0 = H(\eta), \quad \rho/\rho_0 = K(\eta), \quad \frac{dR}{dt} = A. \tag{10}$$

The velocity of the detonation wave is equal to the time-derivative of R i.e. U = dR/dt = A. Integration of the foregoing equation yields R = At, and, consequently, $\eta = r/At$. Introducing now a new variable $\xi = A\eta = r/t$, equations (10) may be rewritten as:

$$u = F(\xi), \quad p/p_0 = H(\xi), \quad \rho/\rho_0 = K(\xi), \quad \frac{dR}{dt} = A.$$

These expressions were employed by G. I. Taylor [3, 14] to solve the problems of the air wave surrounding an

expanding sphere, and the motion of products of an explosion behind spherical detonation waves in solid explosives.

(ii) Spherical blast wave resulting from point-source: Since the blast wave is spherically symmetric, one can put B = G = 0 and R = R(t). Assuming $\ell = 0$ and n = 3/2, equations (9) reduce to

$$u = R^{-3/2} F(\eta) \;,\; p/p_0 = R^{-3} H(\eta),$$

$$\rho/\rho_0 = K(\eta) \;,\; \frac{dR}{dt} = AR^{-3/2}. \qquad (11)$$

This set of transformations was first used by G. I. Taylor [6] to reduce the system of partial differential equations of fluid flow to a system of ordinary ones.

Examination of equations (9) reveals several extremely interesting features. Any arbitrary selection of ℓ and n based upon the physical nature of the problem yields a new set of transformations. A still more remarkable property of equations (9) is the fact that u and v are attenuated with R as the shock head velocity $\partial R/\partial t$ - a result upheld and suggested by intuition.

Also, if ℓ is taken to be zero, the pressure attenuates with R as the square of the velocity of u or v.

Attention will now be directed to transforming the partial differential equations (1-4) to ordinary differential equations for the problem at hand. If ℓ = 0 the substitution of (9) in (1-4) yields:

$$-A\eta K'/K + 2F/\eta + F' + FK'/K + \frac{1}{\eta}\left[-GB\eta\, K'/K - B\eta G' - \eta BG + G\cot\theta\right] = 0 \tag{12}$$

$$-A\left[nF + \eta F'\right] + FF' + \frac{G}{\eta}\left[-nBF - B\eta F'\right] - G^2/\eta = -\frac{c_o^2}{\gamma_o K} H' \tag{13}$$

$$-\left[n + \eta G'/G\right]\cdot\left[A + BG/\eta\right] + F\left[G'/G + 1/\eta\right] = \frac{c_o^2}{\gamma_o K \eta G}\left[2nBH + B\eta H'\right] \tag{14}$$

$$\left[\gamma\eta K'/K - 2n - \eta H'/H\right]\cdot\left[A + BG/\eta\right] + F\left[H'/H - \gamma K'/K\right] = 0 \tag{15}$$

It is useful at this point to make the equations dimensionless. This eliminates A from the equations (12-15). Introduce the following nondimensional variables:

$$f = \frac{F}{A} \;,\; g = \frac{G}{A} \;,\; h = \frac{C_o^2}{A^2} H \;,\; k = K \tag{16}$$

Substitution of (16) in equations (12-15) yields:

$$-\eta k'/k + 2f/\eta + f' + fk'/k + 1/\eta \cdot [-gB\eta \cdot k'/k - B\eta g' - nBg + g\cot\theta] = 0 \tag{17}$$

$$-[nf + \eta f'] + ff' + \frac{g}{\eta}[-nBf - B\eta f'] - g^2/\eta = -\frac{1}{k\,\tilde{\nu}_o} h' \tag{18}$$

$$-[n + \eta g'/g] \cdot [1 + Bg/\eta] + f[g'/g + 1/\eta] = 1/\tilde{\nu}_o \eta k g [2nBh + B\eta h'] \tag{19}$$

$$[\gamma \eta k'/k - 2n - \eta h'/h] \cdot [1 + Bg/\eta] + f[h'/h - \gamma k'/k] = 0 \tag{20}$$

The solution of equations (17-20) in conformity with a suitable set of initial and boundary conditions should give the flow field between the origin and the shock wave. A numerical solution of these equations will be the next objective in the investigation. However, before doing this, it is necessary to pause to examine the question of initial and boundary conditions.

A preliminary examination of Euler's equations (1-4) reveals that one must require for $t > 0$: $v\big]_{\theta=0} = 0$, since otherwise the last term in equation (1) would become infinite. Further the normal component of velocity along the diaphragm, i.e. v, must vanish. More precisely, for $t > 0$ this condition can be formulated $v\big]_{\theta=\pi/2-\epsilon} = 0$, where $\epsilon \to 0$ as the thickness of diaphragm approaches zero. In the limiting case, therefore, this condition may be replaced by $v\big]_{\theta=\pi/2} = 0$. Also u and v must vanish at $r = 0$. Thus, the natural boundary conditions for u and v are:

$$t > 0, \begin{cases} \theta = 0 \\ \theta = \pi/2 \end{cases} : v = 0 \qquad (21)$$

$$t > 0, \; r = 0 : \; u = v = 0 \qquad (22)$$

Integration of equations (17-20) can be carried out numerically step by step if for any value of the variable "η", the functions f, g, h and k are known. It is not, however, feasible to start from the origin as the substitution of (21-22) in (17-20) reveals that $f'(0)$, $g'(0)$, $h'(0)$ and $k'(0)$ become infinite there. Therefore, the integration must be started from a point other than the origin, e.g. the shock head.

Any specification of the boundary conditions at the shock head requires a knowledge of the shock surface shape. It seems reasonable to assume that the shock surface is a function of both θ and t and that $R = R(\theta, t)$ gives any point on the shock surface. Also, then $B(\theta) = 1/R \, \partial R/\partial\theta$ may be calculated. Next the procedure for obtaining values of f, g, h and k at $r = R(\theta, t)$ i.e., $\eta = 1$, will be outlined.

Now the Rankine-Hugoniot conditions at the shock front ($\eta = 1$) are:

$$\rho_1 (U - u_1) = \rho_0 U$$

$$p_1 + \rho_1 (U - u_1)^2 = p_0 + \rho_0 U^2$$

$$\frac{\gamma}{\gamma - 1} \cdot \frac{p_1}{\rho_1} + \frac{1}{2} (U - u_1)^2 = \frac{\gamma_0}{\gamma_0 - 1} \cdot \frac{p_0}{\rho_0} + 1/2 \, U^2,$$

where U is the shock-front speed, and subscripts 1 and 0 denote the quantities immediately behind and in front of the shock wave respectively. However, these conditions cannot be satisfied consistently with similarity assumptions [6]. Nevertheless, these may be replaced by the conditions for strong shock waves when p_1/p_0 is very large. Thus,

$$\rho_1/\rho_0 = (\gamma+1)/(\gamma-1)$$
$$U^2/c_0^2 = (\gamma+1)/2\gamma_0 \quad \chi$$
$$u_1/U = 2/(1+\gamma)$$

where $\chi = p_1/p_0$ and $\vec{u}_1 = \vec{e}_r\, u(1) + \vec{e}_\theta\, v(1)$. $\vec{e}_r$ and $\vec{e}_\theta$ designate unit base vectors along the directions of increasing r and θ respectively. These relations are also valid when γ is replaced by $\bar{\gamma}$ (see Reference 15).

Under the general transformations (9), these boundary conditions reduce to the following:

$$h^*(1) = \frac{2\gamma_0}{\gamma+1}\,(A/c_0)^{-1/n} R^l$$
$$k^*(1) = \frac{\gamma+1}{\gamma-1}\,(A/c_0)^{-1/n} R^l$$
$$\omega^*(1) = \frac{2}{1+\gamma}$$

(23)

with

$$\vec{\omega}^*(1) = \vec{e}_r f^*(1) + \vec{e}_\theta g^*(1) \ , \ |\vec{\omega}^*(1)| = \omega^*(1)$$

Hence

$$f^*(1) = \frac{2}{1+\gamma} \cos\lambda \ , \ g^*(1) = \frac{2}{1+\gamma} \sin\lambda \tag{24}$$

where λ is the angle between the radius vector and the normal to the shock surface R = R(θ, t). Note that f^*, g^*, h^*, k^* are nondimensional quantities, but not necessarily the same as f, g, h, and k. In fact, they are related to dimensional quantities in the following manner:

$$f^* = F/A \ , \ g^* = G/A \ , \ h^* = (A/c_0)^{-\frac{l-2n}{n}} \cdot H$$
$$k^* = (A/c_0)^{-l/n} \cdot K \tag{25}$$

The relations (23) represent the boundary conditions for the equations of flow which have been transformed to ordinary differential equations under the generalized similarity transformations (9). It is seen from equations (23) that unless l = 0, boundary conditions vary with R, thus contradicting the similarity hypothesis. Hence, to satisfy the similarity hypothesis l must be zero.

This is, of course, what was assumed earlier. When $\ell = 0$, equations (25) become identical with equations (16). Hence f^*, g^*, h^* and k^* become also identical with the corresponding unstarred variables. Consequently from equations (23), the boundary conditions for (17-20) are:

$$\eta = 1: \quad h = \frac{2\gamma_0}{1+\gamma}, \quad k = \frac{\gamma+1}{\gamma-1},$$

$$\omega = \frac{2}{1+\gamma} \tag{26}$$

where

$$\vec{\omega} = \vec{e}_r f(1) + \vec{e}_\theta g(1), \quad |\vec{\omega}| = \omega.$$

Before proceeding further, a few remarks concerning the calculation of "A" seem to be in order.

The total energy E of the disturbance consists of two parts, the kinetic energy

$$8 \int_0^{\pi/2} \int_0^R 1/2 \rho (u^2 + v^2) r^2 \, dr \, d\theta$$

and the heat energy

$$8 \int_0^{\pi/2} \int_0^R \frac{p r^2}{\gamma - 1} \, dr \, d\theta$$

Therefore

$$E = 4 \rho_0 A^2 \left[\int_0^{\pi/2} R^{3-2n} \int_0^1 k (f^2 + g^2) \eta^2 \, d\eta \, d\theta + \frac{2}{\gamma_0} \int_0^{\pi/2} R^{3-2n} \int_0^1 \frac{h \eta^2}{\gamma - 1} \, d\eta \, d\theta \right] \tag{27}$$

Since it is simpler to consider a spherically symmetric case, attention shall be devoted in the following primarily to it. Of course, it goes without saying that the remarks below will apply equally to the axisymmetrical case. For a spherically symmetric shock-wave, equation (27) reduces to:

$$E = 2\pi \rho_0 A^2 R^{3-2n} \left[\int_0^1 k f^2 \eta^2 d\eta + \frac{2}{\gamma_0} \int_0^1 \frac{h \eta^2}{\gamma - 1} d\eta \right] \tag{28}$$

From this relation it is clear that unless $n = 3/2$, E depends explicity on R($E \propto R^{3-2n}$) and hence through it implicitly on time t. The case $n = 3/2$ corresponds to the point source finite energy explosion.

The problem that now faces one is "what happens when $n \neq 3/2$ and lies between $0 \leqslant n < 3/2$ i.e. for short moments immediately after explosion?"

E must equal the energy of chemical explosion, and at the same moment must depend upon t if similarity relations are to be satisfied. This point has also been discussed by H. Morgenroth [16] and M. H. Rogers [17]. At this point, it is instructive to examine the physical nature of the blast wave generated by a finite source.

Flow behind the leading shock in this case is not continuous [13, 18].

The explosive gases behave like a piston and feed energy into the ambient gases behind the main shock-front. The piston surface is a contact surface. Besides the contact surface, there must occur additional shocks as shown in Figure 2. Initially, contact surface and leading shock are together and region I is non-existent. However, later on as ambient gases are absorbed by the blast wave, region I develops.

It is essential to find, therefore, three separate solutions. The method outlined here can only be used to find solution in region I. The solution cannot be extended beyond the contact surface and hence it is not possible to satisfy the inner boundary condition of zero velocity at the center. Thus in region I, the relation $E_I \propto R^{3-2n}$ is satisfied. Theoretically, then, by changing limits of integration in equation (28) so as to include only region I, it should be possible to calculate A. This, however, requires finding solutions for regions II and III as well. The energy in all three regions equals total energy (E). Since, however, it is not possible to apply similarity solution to regions II and III, it is now necessary to

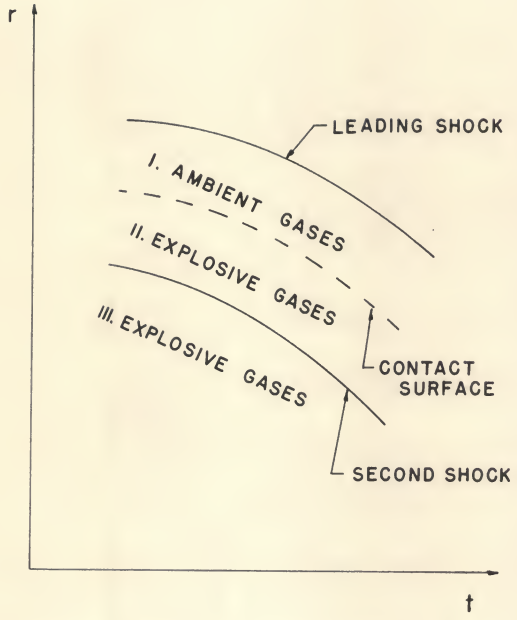

Figure 2: Flow behind the Main Shock

abandon the equation of energy to determine "A". A must be found from experimental data concerning the time history of shock propagation.

3. Numerical Calculations for Spherical Blast Waves

In this section it is proposed to provide a solution for the spherical blast waves resulting from both the finite source and point source explosions. In Section I certain previous theoretical as well as experimental results were reviewed. On the basis of these, it is possible to apply different similarity solutions for different times.

The equations of motion in dimensionless form are obtained from equations (17-20) by ignoring the θ coordinate. These may be written after some elementary algebraical manipulations as:

$$\frac{h'}{h}\left[\frac{(\eta-f)^2}{\gamma} - \frac{h}{\gamma_0 k}\right] = f\left[\frac{2n}{\gamma} - n + 2\right] - 2f^2/\eta - 2n\eta/\gamma \qquad (29)$$

$$f' = \frac{2n}{\gamma} + \frac{h'}{\gamma h}(\eta - f) - 2f/\eta \qquad (30)$$

$$k' = \frac{h'k}{\gamma h} + \frac{2nk}{\gamma(\eta - f)} \qquad (31)$$

where γ and γ_o denote the values of the ratio of specific heats behind and in front of the shock wave, respectively.

It will be assumed in the following that for small times the pressure behind the shock front is considerably greater than in front of it in order to justify the use of strong shock boundary conditions. From equation (26), the boundary conditions at $\eta = 1$ are:

$$f = \frac{2}{1+\gamma} \quad , \quad k = \frac{\gamma+1}{\gamma-1} \quad , \quad h = \frac{2\gamma_o}{1+\gamma} \tag{32}$$

The solution of equations (29-31) subject to the conditions (32) can be carried out only by numerical means.

The numerical method employed to solve equations (29-31) is a special form of the Runge-Kutta method, due to Merson [19]. The differential equations (29-31) were programmed on the IBM 709 computer, utilizing the numerical method mentioned above to yield results for various values of n, within three per cent accuracy at each step. The integration interval employed was w = 0.002 (except in Case 3). Results have been obtained for the following cases:

Case 1

$$\gamma = \gamma_0 = 1.4 \quad , \quad n = 0.5$$

Behavior of compressed ambient gas region for short times after explosion.

Case 2

$$\gamma = \gamma_0 = 1.4 \, , \quad n = 1.0$$

Same as in Case 1 expect in so far as it relates to intermediate values of time.

Case 3

$$\gamma = \gamma_0 = 1.4 \, , \quad n = 1.5$$

The integration interval employed was 0.01. This is identical with Taylor's finite-energy point source explosion solution. In Table 1, the solution given by Taylor [6] is compared to the one obtained here. The other results of these computations are reproduced in Figures 3-5.

If one regards the contact surface as the outer boundary of an expanding sphere of radius (r), then its velocity is given by (see Reference 14):

$$u = \frac{r}{R} \frac{dR}{dt} = \eta U$$

TABLE 1

SPHERICAL SYMMETRIC POINT SOURCE EXPLOSION:
COMPARISON OF TAYLOR'S [6] RESULTS
WITH THE AUTHOR'S

	h		f		k	
η	Taylor Solution	Present Solution	Taylor	Present	Taylor	Present
1.00	1.167	1.167	0.833	0.833	6.000	6.000
0.98	0.949	0.955	0.798	0.798	4.000	4.068
0.96	0.808	0.813	0.767	0.766	2.808	2.887
0.94	0.711	0.714	0.737	0.736	2.052	2.122
0.92	0.643	0.644	0.711	0.709	1.534	1.603
0.90	0.593	0.592	0.687	0.684	1.177	1.235
0.88	0.556	0.553	0.665	0.661	0.919	0.967
0.86	0.528	0.524	0.644	0.639	0.727	0.765
0.84	0.507	0.502	0.625	0.611	0.578	0.619
0.82	0.491	0.484	0.607	0.600	0.462	0.490
0.80	0.478	0.471	0.590	0.582	0.370	0.395
0.78	0.468	0.460	0.573	0.565	0.297	0.319
0.76	0.461	0.452	0.557	0.548	0.239	0.257
0.74	0.455	0.446	0.542	0.532	0.191	0.208
0.72	0.450	0.441	0.527	0.516	0.152	0.168
0.70	0.447	0.437	0.513	0.501	0.120	0.135
0.68	0.444	0.434	0.498	0.485	0.095	0.108
0.66	0.442	0.432	0.484	0.463	0.074	0.086
0.64	0.440	0.430	0.470	0.455	0.058	0.068
0.62	0.439	0.429	0.456	0.441	0.044	0.054
0.60	0.438	0.428	0.443	0.426	0.034	0.042
0.58	0.438	0.427	0.428	0.419	0.026	0.033
0.56	0.437	0.426	0.415	0.396	0.019	0.025
0.54	0.437	0.426	0.402	0.382	0.014	0.019
0.52	0.437	0.425	0.389	0.367	0.010	0.015
0.50	0.436	0.425	0.375	0.352	0.007	0.011
0.45		0.425		0.315		0.005
0.40		0.425		0.278		0.002
0.35		0.425		0.240		0.001
0.30		0.425		0.201		0.000
0.25		0.425		0.159		0.000
0.20		0.425		0.132		0.000
0.15		0.425		0.053		0.000
0.12		0.425		0.001		0.000
0.00*		0.425		0.000		0.000

*This entry was extrapolated.

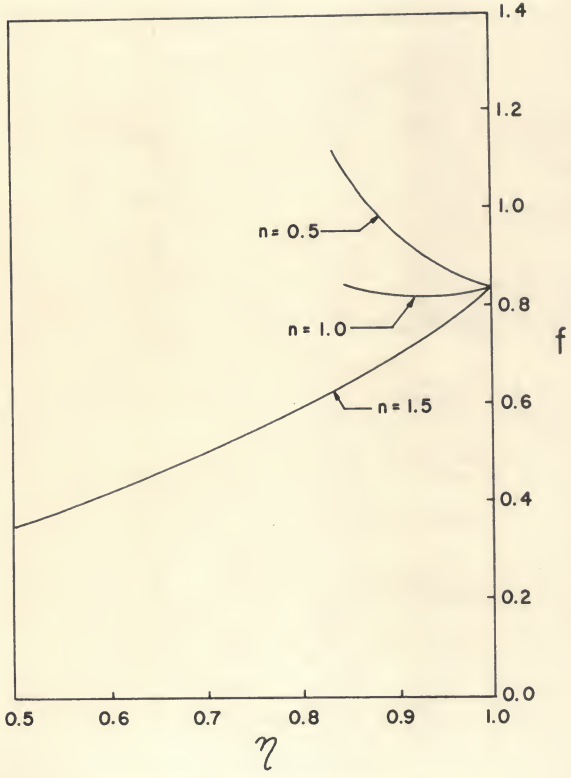

Figure 3: Plot of f Versus η

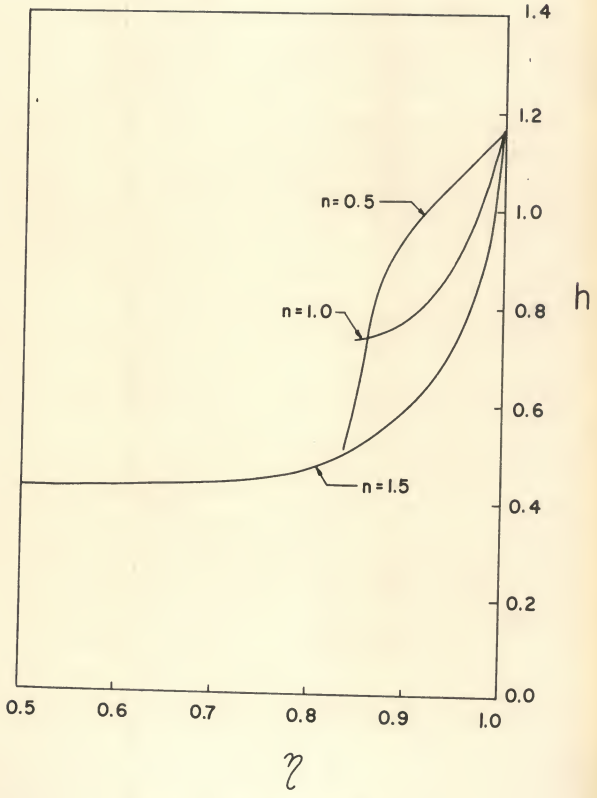

Figure 4: Plot of h versus η

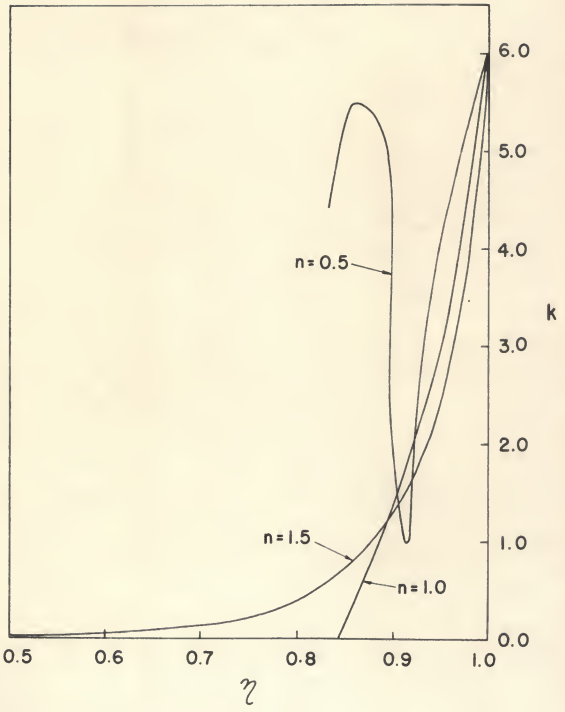

Figure 5: Plot of k versus η

Also from equations (9) and (16),

$$u = U f(\eta)$$

Comparing the two relationships, the contact front is defined by

$$\eta = f(\eta)$$

Thus for the Cases 1 and 2, the contact front is specified by

Case 1 $\eta = f = 0.915$

Case 2 $\eta = f = 0.846$

Evidently, any solution beyond these points is not physically realistic.

It was shown previously that for finite source explosions, the calculation of "A" must be made from experimental results. Hence, it is not possible here to cite any results for Cases 1 and 2. "A" can be determined in these cases in the following manner. From Schlieren photographs, it is possible to obtain the velocity of propagation U of the main shock. Once U is known, A may be obtained by application of the formula $U = AR^{-n}$. Experimental investigations along these lines are reported in Chapter II.

The situation is different with regard to Case 3. Here, equation (28) reduces to the following simple form:

$$E = 2\pi \rho_0 A^2 \left[\int_0^1 \left(k f^2 \eta^2 + \frac{2}{\tilde{r}_0} \cdot \frac{h \eta^2}{r-1} \right) d\eta \right]$$

Numerical integration yields

$$E = 5.38\, A^2 \rho_0$$

Compare this to the values obtained by G. I. Taylor [6]. His computations show that $E = 5.36\ \rho_0 A^2$ and thus are in quite remarkable agreement with present results. D. L. Jones [20] gives a slightly different value ($E = 5.33\ \rho_0 A^2$). Finally, given E and ρ_0, A may be evaluated.

4. Numerical Calculations for Axisymmetrical Point-Source-Finite-Energy Blast Wave

The equations of motion (17-20) may be written in a form more suitable for numerical procedure as follows:

$$h' \left[-\frac{\eta \sigma}{r h} + \frac{\eta}{k \tilde{r}_0 \sigma} (1 + B^2) \right] = n B g - g \cot\theta - 2f + B f g/\sigma - \frac{B^2}{\tilde{r}_0 k \sigma}\, 2 n h + g^2/\sigma + n(\sigma + f)(2/r - B g/\sigma + f/\sigma)$$

(33)

$$f' = \frac{(\eta/k\tilde{r}_0) h' - g^2 - n f (\sigma + f)}{\eta \sigma}$$

(34)

$$g' = \frac{fg - ng(\sigma + f) - \frac{B}{\gamma_0 k}(2nh + \eta h')}{\eta \sigma} \tag{35}$$

$$k'/k = \frac{2n(\sigma + f) + \eta \sigma h'/h}{\gamma \sigma \eta} \tag{36}$$

where

$$\sigma = \eta + Bg - f$$

Also, from equations (24) and (26), the boundary conditions at η = 1 are:

$$f = \frac{2}{1+\gamma} \cos\lambda \quad , \quad g = \frac{2}{1+\gamma} \sin\lambda$$

$$h = \frac{2\gamma_0}{1+\gamma} \quad , \quad k = \frac{\gamma + 1}{\gamma - 1} \tag{37}$$

The numerical technique employed in the programming of equations (33-36) for solution on IBM 709 Computer was the same as described in Section 3. Also, the same integration interval w = 0.002 was employed.

It is assumed that the explosion is due to a point source in air. Therefore, γ, γ_0 and n have the values 1.200, 1.200 and 1.500, respectively.

To preform numerical calculations, it is necessary to specify $R(\theta, t)$ at some moment so as to make the calculation of $B(\theta)$ and λ feasible. It may happen in an actual problem that B depends on t as well. In this case, it will be necessary to specify the shape of the shock wave $R(\theta, t)$ throughout the time interval. The similarity solution may be applied now by approximating B in a short time interval Δt, so that B depends essentially on θ only. This, though interesting will not be pursued further in the following.

While the exact shape of the shock head must be determined experimentally, it was thought fit to examine here the hypothetical case when the shock head happens to be an ellipsoid of revolution. This can be done if one assumes that the ellipsoid of revolution approximates the shock surface in a short-time interval Δ t. A cross-sectional view is given in Figure 6. The equation of an ellipse can be written in the form

$$R^2 = \frac{R_o^2 (R_o - \delta)^2}{R_o^2 \sin^2\theta + (R_o - \delta)^2 \cos^2\theta} \qquad (38)$$

where $R = R(\theta, t)$ denotes the radius of the shock head, R_o the semi-major axis, and $R_o - \delta$ the semi-minor axis.

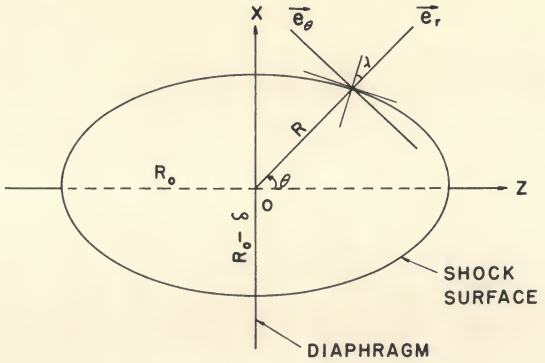

Figure 6: Sketch of Axisymmetric Shock Surface

Clearly R_o and $R_o - \delta$ are functions of time. Then, from equations (38)

$$B = \frac{1}{R}\frac{\partial R}{\partial \theta} = \frac{SIN\,\theta\,COS\,\theta\,[(R_o-\delta)^2 - R_o^2]}{(R_o-\delta)^2 COS^2\theta + R_o^2 SIN^2\theta}$$

$$\lambda = ARC\ TAN(-B) = -B \qquad (39)$$

The calculations were conducted for the special case when $R_o = 2.2$ and $R_o - \delta = 2$ (Units are not important. It is only the ratio $R_o/R_o-\delta$ that matters.) Then $B(\theta)$, f(l) and g(l) can be calculated from equations (39). Below are tabulated some of these values:

TABLE 2

B, f AND g AS FUNCTIONS OF θ

	$\frac{R_o}{R_o-\delta} = \frac{2.2}{2} = 1.1$		
θ	$B(\theta)$	f(l)	g(l)
0°, 90°	-0.000	0.9091	0.0000
30°	-0.162	0.9057	0.0783
60°	-0.154	0.9063	0.0712

The differential equations were solved for these particular values of θ. Results are reproduced in Table 3. Some explanatory notes are required to fully comprehend Table 3. These comments may be divided into two parts, i.e., concerning calculations for

TABLE 3

NUMERICAL RESULTS FOR AXISYMMETRICAL
Case $[\gamma - \gamma_0 = 1.2, n = 1.5]$

η \ θ	h			k			f			g		
	0°,90°	30°	60°	0°,90°	30°	60°	0°,90°	30°	60°	0°,90°	30°	60°
1.000	1.091	1.091	1.091	11.000	11.000	11.000	0.909	0.906	0.906	0.000	0.078	0.071
0.990	0.924	0.937	0.934	7.384	7.235	7.261	0.889	0.894	0.893		0.050	0.044
0.980	0.811	0.834	0.830	5.226	4.988	5.037	0.870	0.884	0.882		0.020	0.016
0.974	0.759	0.789	0.784	4.330	4.058	4.116	0.860	0.879	0.875		0.001	0.001
0.970	0.730	0.763	0.757	3.845	3.554	3.617	0.853	0.873	0.869		.	
0.960	0.672	0.711	0.704	2.912	2.596	2.667	0.837	0.861	0.856			
0.950	0.628	0.673	0.665	2.255	1.933	2.005	0.822	0.849	0.844		Terminated	
0.900	0.518	0.588	0.575	0.758	0.500	0.555	0.761	0.802	0.794		(It is now	
0.850	0.482	0.568	0.551	0.290	0.126	0.156	0.712	0.763	0.754		necessary to	
0.800	0.468	0.563	0.545	0.113	0.026	0.038	0.668	0.728	0.717		put g = 0	
0.750	0.464	0.562	0.544	0.042	0.004	0.007	0.625	0.695	0.682		This reduces	
0.700	0.462	0.562	0.543	0.015	0.000	0.001	0.583	0.664	0.649		number of	
0.650	0.462	0.562	0.543	0.005	0.000	0.000	0.541	0.633	0.618		differential	
0.624	0.462	0.562	0.543	0.003	0.000	0.000	0.519	0.622	0.603		equations to	
0.600	0.461		0.543	0.002		0.000	0.499		0.589		three)	
0.584	0.461		0.543	0.001		0.000	0.486		0.581			
0.550	0.461			0.000			0.457					
0.500	0.461	Terminated		0.000	Terminated		0.415	Terminated				
0.400	0.461			0.000			0.331	($f \approx \eta$ may				
0.300	0.461			0.000			0.246	be used to				
0.200	0.461			0.000			0.158	approximate				
0.100	0.461			0.000			0.049	solution in				
0.074	0.461			0.000			0.001	this region)				
*0.000	0.461	0.562	0.543	0.000	0.000	0.000	0.000	0.000	0.000	0.000	0.000	0.000

Terminate integration here

*Values extrapolated.

(a) $\theta = 0^\circ, 90^\circ$

and

(b) $\theta = 30^\circ, 60^\circ$

$\underline{\theta = 0^\circ, 90^\circ}$

In this case, B = g = 0 and consequently the system of equations (33-36) becomes identical with that for spherically symmetrical shock waves. Calculations can be carried on to rather low values of η (≈ 0.1), when the accumulated error necessitates approximation. Since this has already been covered in Section 3, nothing more need be said here.

$\underline{\theta = 30^\circ, 60^\circ}$

The numerical calculations in this case are to be carried out in three essential steps. First, the system (33-36) is examined. The solution can be carried out up to $\eta = 0.974$, when the small value of g makes it necessary to change the numerical procedure (if this is not done, there results an error in the value of g of its own order). In the second step, g is put equal to zero. This means equation (35) drops out and system (33-36) becomes identical with that for the symmetrical case. This approximation allows the solution up to the point $\eta \approx 0.6$. At this point, however, $k \approx 0$ and h

approaches a constant value. f must approach zero at $\eta = 0$. Between $\eta \approx 0.6$ and $\eta = 0$, $f \approx \eta$ provides a good approximation. Also, around $\eta \approx 0.6$, k' becomes small such that it may be neglected. Then the approximation $f = \eta$, yields

$$h' = 3/2\ \gamma\ \eta\ k$$

The calculation of A is straightforward in this case as E = const (Section 2). Evaluation of the integral (27) leads to the result

$$E = 11.537\ \rho_0\ A^2$$

Hence given the values of ρ_0 and E, A may be found. Calculations have also been carried out for the case when $\gamma = \gamma_0 = 1.4$ and $n = 1.5$. These are reproduced in Table 4. Here

$$E = 5.591\ \rho_0\ A^2$$

5. Conclusions

The existence of a general set of similarity transformation for the axisymmetrical Euler equations (in spherical coordinates) has been shown. Previous similarity solutions of Taylor [3, 6, 14] have been demonstrated to be special cases of these transformations. It is not possible to satisfy the exact Rankine-Hugoniot conditions at the shock-front. However, the conditions

TABLE 4

NUMERICAL RESULTS FOR AXISYMMETRICAL
CASE [$\gamma = \gamma_o = 1.4$, $n = 1.5$]

$\eta \downarrow$ $\theta \rightarrow$	h			k			f			g		
	0°,90°	30°	60°	0°,90°	30°	60°	0°,90°	30°	60°	0°,90°	30°	60°
1.000	1.167	1.167	1.167	6.000	6.000	6.000	0.833	0.830	0.831	0.000	0.072	0.065
0.990	1.045	1.059	1.057	4.908	4.905	4.905	0.815	0.818	0.817		0.056	0.050
0.980	0.955	0.972	0.968	4.068	4.054	4.057	0.798	0.807	0.805		0.034	0.034
0.970	0.877	0.900	0.896	3.410	3.382	3.389	0.782	0.796	0.793		0.021	0.017
0.960	0.813	0.841	0.836	2.887	2.845	2.856	0.766	0.786	0.782		0.003	0.000
0.958	0.802	0.831	0.825	2.796	2.750	2.763	0.763	0.784	0.780		0.000	
0.950	0.759	0.791	0.784	2.466	2.407	2.422	0.751	0.774	0.769		Terminated	
0.900	0.592	0.636	0.627	1.235	1.135	1.157	0.684	0.719	0.713		(It is now	
0.850	0.512	0.567	0.556	0.683	0.572	0.596	0.629	0.677	0.668		necessary to	
0.800	0.471	0.535	0.522	0.395	0.287	0.309	0.582	0.643	0.632		put g = 0	
0.750	0.449	0.520	0.506	0.232	0.136	0.154	0.540	0.614	0.601		This reduces	
0.700	0.437	0.514	0.498	0.135	0.057	0.070	0.501	0.588	0.573		number of	
0.650	0.431	0.511	0.495	0.077	0.019	0.027	0.463	0.567	0.548		differential	
0.600	0.428	0.511	0.495	0.042	0.004	0.008	0.426	0.548	0.528		equations to	
0.550	0.426	0.511	0.494	0.022	0.000	0.001	0.389	0.536	0.510		three)	
0.536	0.426	0.511	0.494	0.018	0.000	0.000	0.379	0.533	0.506			
0.502	0.425		0.494	0.011		0.000	0.354		0.499			
0.500	0.425	Terminated		0.011	Terminated		0.352	Terminated				
0.400	0.425			0.002			0.278	(f ≈ 7 may				
0.300	0.425			0.000			0.201	be used to				
0.200	0.425			0.000			0.112	approximate				
0.168	0.425			0.000			0.079	solution in				
								this region)				
*0.000	0.425	0.510	0.494	0.000	0.000	0.000	0.000	0.000	0.000	0.000	0.000	0.000

Same throughout the interval

*Values extrapolated

at the shock front can be satisfied under strong shock assumptions.

When the source of blast wave is finite, it is not possible to use the energy relationship to solve the problem completely. Despite this difficulty, the method has been demonstrated to be capable of providing approximate solutions in such cases, when information on time-history of the shock front is available. Finally, it is possible to apply this method to analyze the problems of axisymmetric blast waves. In this instance, however, one must require additional information about the shape of the shock-head.

CHAPTER II

SOME EXPERIMENTAL RESULTS FOR BLAST WAVES ORIGINATING FROM A FINITE SOURCE

1. Introduction

In Chapter I a similarity solution has been obtained for the compressed air region between the main shock and the contact surface in a spherically symmetric blast wave generated by a finite charge. It was pointed out that in order to complete the solution, it is necessary to determine a certain constant "A" from experimental data. Once "A" is known, it is possible to find the pressure, density and velocity distribution behind the main shock. The most convenient way to evaluate "A" is to first find "U" - the main shock velocity - from Schlieren pictures, and then apply the relation $U = AR^{-n}$, where R is the shock wave radius and n is a constant. In this Chapter a method employing a multi-spark camera for obtaining the Schlieren record is presented. Also, two examples for very short-time following the explosion are given.

2. Equipment and Procedure

The multi-source spark camera is of the so-called Cranz-Schardin type [21], and was first developed at the National Physical Laboratory (NPL), England [22]. Reference [23] describes a modified version of the NPL model, being used at the University of Toronto Institute of Aerospace Studies, Canada, for visualizing flow behind a blast wave. The camera and the auxiliary system (Figure 7) employed at the University of Florida is basically the same as the one used at UTIAS.

The camera essentially consists of a number of individual Schlieren systems. It makes use of a pair of common main mirrors and groups of distinct but identical light sources, lenses and knife edges. Each separate Schlieren system is triggered at a predetermined time from an initial pulse originating from the flow phenomenom to be observed. In the present case, a given flow is visualized from five slightly different angles and recorded as five different distinct photographic images on a single sheet of film. The time between exposures can be varied by means of short-duration pulse techniques and time-delay units, from a minimum of 2 μseconds upwards. The chief disadvantage of this camera is the

Figure 7: Test Stand

limited number of pictures. However, as pointed out in Reference 23 , this disadvantage is offset by the simplicity of design, economy, resolution, pre-set variable or constant framing rate to suit a given experiment.

Two different sizes of uncased PBRDX charge were employed in the testing program i.e., (1) a spherical charge of 3/8 inch diameter varying in weight from 0.56 grams to 0.62 grams and (2) a spherical charge of 1/2 inch diameter varying in weight from 1.27 grams to 1.31 grams. These charges were detonated by use of a high-energy blast cap activated by a one microfarad 5000 volt condenser.

The time delay unit was set to trigger the first spark source after 4.3 microseconds of the initiation of the blast cap. Succeeding frames were taken at 7, 10, 15 and 20 microseconds, respectively. This sequence was adhered to throughout the entire experimental program to obtain reproducible results. Figure 8 reproduces a typical firing.

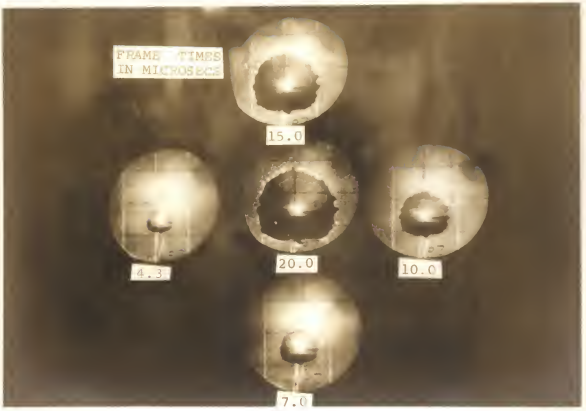

Figure 8: A Typical Firing Sequence for 0.6 gm PBRDX Charge

3. Experimental Results

A close look at Figure 8 shows that for very short times immediately following the explosion such as in the present case, the second shock has not still separated from the contact surface. There is a very thin compressed air region. This phenomenon was previously observed by H. Schardin [24]. Another remarkable feature is the irregularity of the outer boundary of the expanding explosive gases. The flat region from which two wires protrude is due to the effect of the nonsymmetrical explosion of the blast cap.

To find the shock wave radius R as a function of time t, it was found necessary to approximate the irregular material boundary by a circle. Also, the flat region was neglected. R was read to within 0.5 mm. (scale 3.60 cm = 2 inches) from the pictures. The values for R are given in columns 2-4 (0.6 gm charge) and columns 6-8 (1.3 gm charge) of Table 5. Then the velocity U = (dR/dt) of the shock-head was determined by approximating the differential quotient dR/dt by the difference quotient:

$$U_{i+1/2} = \frac{R_{i+1} - R_i}{t_{i+1} - t_i} ,$$

TABLE 5

EXPERIMENTAL RESULTS FOR FINITE
ENERGY BLAST WAVES

Charge size	0.6 gm				1.3 gm			
Time (μsec)	R (inches)				R (inches)			
	Test 1	Test 2	Test 3	R cal	Test 1	Test 2	Test 3	R cal
4.3	0.778	0.722	0.750	0.750	0.828	0.828	0.828	0.828
7.0	1.166	1.166	1.166	1.171	1.242	1.242	1.242	1.273
10.0	1.444	1.500	1.444	1.516	1.587	1.587	1.587	1.663
15.0	1.916	2.000	1.945	1.970	2.139	2.174	2.208	2.200
20.0	2.305	2.356	2.332	2.357	2.622	2.691	2.622	2.658
	$A = 150 \times 10^{-3}$ units* $n = 0.89$				$A = 170 \times 10^{3}$ units* $n = 0.70$			

*System of units used consists of inches, seconds and grams.

with
$R_i = R(t_i)$, $R_{i+1} = R(t_i + 1)$, $U_{i+1/2} = U(t_i + 1/2\,\Delta t)$
and $t_{i+1} = t_{i+\Delta t}$, $i = 1, 2, \cdots$

These values of U are plotted (see Figure 9) on a log-log paper. The experimental points show an even scatter around a straight line. If one now applies the formula: $U = AR^{-n}$, the values of A and n may be directly read from the graph. (Regarding the R-axis as the abscissa and the U-axis as the ordinates, n is simply the slope of the straight line. The value of A equals U at R = 1 inch.)

In order to check the accuracy of the straight-line approximation, R was calculated by using the formula

$$R = \left[A(t - t_o)(n + 1) + R_o^{n+1}\right]^{1/n+1}$$

(this formula can be easily obtained by integrating the equation

$$U = \frac{dR}{dt} = A R^{-n}$$

within the limits t_o, R_o and t, R) where t_o and R_o correspond to the first frame. The calculated values of R are given in columns 5 (0.6 gm charge) and 9 (1.3 gm charge) of Table 5. They differ by less than five per cent from observed values of R - an extremely good agreement in view of the inaccuracies in reading the values of R from the pictures. The values for U can be extrapolated

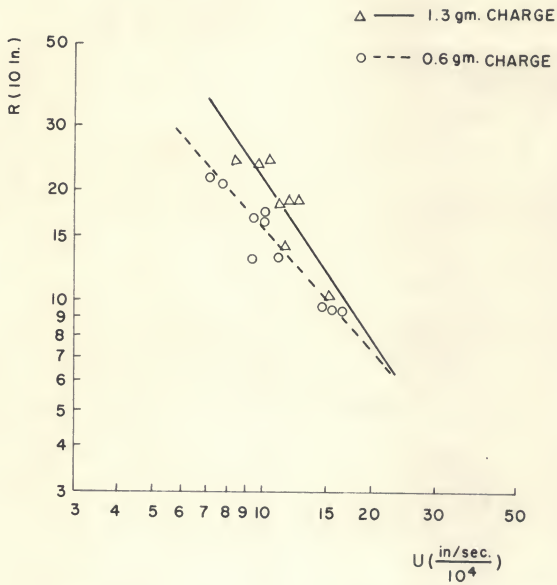

Figure 9: Variation of Shock Head Velocity with Shock Radius

from the experimental curves by simply extending the curves. Care must be taken in doing this. U can be approximated in this manner to approximately R = 0.5 inch on the lower side. For values smaller than R = 0.50 inch, the approximation is bound to be unreliable as at this point the shock-head velocity U becomes equal for both small and large charges. Similarly on the upper end, it does not seem possible to extrapolate beyond R = 2.50 inches due to low overpressures.

4. Expansion of Explosion Products

The treatment here follows closely that outlined by Zeldovich and Kompaneets [2]. Given the initial loading density ρ_i of the solid explosive, it is possible to find the detonation velocity D and the density ρ_d of the explosion products in the detonation front. For the present explosive, with a loading density ρ_i of 1.60 gm/cm^3, the detonation velocity D, the pressure p_d in the detonation front, and the density ρ_d have the values 8000 m/sec, 268.10^3 atm. and 2.17 gm/cm^3 respectively. The explosion products expand in air in essentially two steps:

(i) from (p_d, ρ_d) to (p_x, ρ_x) according to polytropic gas law $p\rho^{-\gamma_1} = \text{const}$ and

(ii) from (P_x, ρ_x) to any lower (P, ρ) according to polytropic equation $P\rho^{-\gamma_2} = \text{const.}$ ($\gamma_2 < \gamma_1$). While use of γ_1 gives appropriate expansion in earlier stages, its use after a certain point tends to give too large an expansion. This necessitates the use of γ_2 ($\gamma_2 < \gamma_1$) to describe the latter stage. The juncture point represents the boundary line between the two stages. The juncture point (P_x, ρ_x) which is of special interest in the expansion of the explosion products in air if found by solving the equations

$$\frac{P_x \rho_x^{-1}}{\gamma_2 - 1} = Q - \frac{D^2}{2(\gamma_1^2 - 1)}$$

and

$$P_x \rho_x^{-\gamma_1} = P_d \rho_d^{-\gamma_1}$$

simultaneously. The heat of explosion is denoted by Q. In the present case, taking Q = 1280 cal/gm, $\gamma_1 = 3$ and $\gamma_2 = 1.3$, (these values are suggested by the given quantities ρ_1 and D. Also see Reference 2) the juncture point (P_x, ρ_x) is found to be

$$P_x = 1580 \text{ atm}$$
$$\rho_x = 0.39 \text{ gm/cm}^3$$

5. Pressure Calculations

From Chapter I, pressure p, density ρ and velocity u behind the main shock in the compressed air region are given by:

$$p = p_0 R^{-2n} A^2 h(\eta)/c_0^2 = p_0 U^2 h(\eta)/c_0^2$$

$$\rho = \rho_0 k(\eta)$$

$$u = U f(\eta)$$

where p_0, ρ_0 refer to values of pressure and density in the ambient atmosphere. In these equations, $\eta = r/R$ denotes a dimensionless similarity variable, where r locates any point in the flow field from the center of the explosion.

For $\eta = 1$ (i.e., just behind the main-shock) under strong shock assumptions h, k and f have the values:

$$h(1) = \frac{2\gamma}{1+\gamma}, \quad k(1) = \frac{\gamma+1}{\gamma-1}, \quad f(1) = \frac{2}{1+\gamma}$$

For the case, $\gamma = 1.2$ i.e., when the equation of state of air is approximated by the law $p\ \rho^{-1.2} = \text{const}$, these values become:

$$h(1) = 1.091, \quad k(1) = 11.000, \quad f(1) = 0.909$$

It is possible to find $h(\eta)$, $k(\eta)$ and $f(\eta)$ in the compressed air region behind the main shock as shown in Chapter I. Also, the contact front may be determined. The contact front is thus specified by:

(a) 0.6 gm. Charge, $\eta = 0.89$

$\eta = f(\eta) = 0.920$, $h(\eta) = 0.748$,

$k(\eta) = 0.023$

(b) 1.3 gm Charge, $\eta = 0.70$

$\eta = f(\eta) = 0.940$, $h(\eta) = 0.831$

$k(\eta) = 0.349$

Across a contact front, pressure (p) and velocity (u) are continuous whereas density (ρ) varies discontinuously. The density across the contact front may, then, be determined from the relation

$$p \rho^{-1.3} = \text{constant}$$

For example at R = 1.25 inches, the pressure and density across the contact front are given by

(a) 0.6 gm. Charge

$\eta = 0.920$: $p = 67$ atm, $\rho = 0.034 \frac{gm}{cm^3}$

(b) 1.3 gm. Charge

$\eta = 0.940$: $p = 100$ atm, $\rho = 0.047 \frac{gm}{cm^3}$

Similar calculations can be performed for other values of R.

CHAPTER III

ON FRACTURE OF A THIN SPHERICAL SHELL UNDER BLAST LOADING

1. Introduction

The behavior of materials under impulsive loading is of great interest in a number of situations. Apart from the military applications (e.g. construction of bombs), it is important in the understanding of various phenomena involving short-time collisions (e.g. meteorite collisions). It has been recognized for a long time that materials under impulsive loading behave in an essentially different manner than in the static situation. In the present work, an experimental investigation was directed towards the study of the fracture pattern and applicability of a modified form of Rinehart and Pearson's criteria. Experiments on thin shells* made of polystyrene plastic revealed the fracture pattern to be primarily of

*Thin shell is defined as the one for which wall thickness is less than 10 per cent of the shell radius.

a brittle type. Also, the critical velocity of straining (V_{cr}) was found to be directly proportional to the cube of the shell diameter. Finally the effect of shell wall thickness and material properties on the number of fragments is examined on the basis of dimensional analysis.

2. Fracture Criteria

The first mathematical treatment of fracture of elastic media was given by A. A. Griffith [25], and was later extended independently to plastic materials by E. Orowan [26] and G. Irwin [27]. This work, however, deals entirely with nonimpulsive loads, and is unsuitable for application to the present case. N. F. Mott [28] made the initial attempt at presenting a rational theory for the fracture of cylindrical ring bombs. He based his development of the theory upon a property of the materials in static tension tests, known as "scatter". Apart from the fact that materials can sustain considerably larger stresses for short periods of time than under static conditions and as such any extension of static results to impulsive situation is uncertain, Mott's theory is dependent upon the following two assumptions i.e., (1) fracture propagation is instantaneous as

compared to rate of strain. (Rate of strain = V/R, where V denotes the particle velocity and R is the radius of the cylinder) (2) fracture occurs due to exhaustion of ductility (in other words, fracture is determined by total strain and not strain rate).

An alternative theory for fracturing of cylindrical shells is presented by J. S. Rinehart and J. Pearson [29]. Although this theory agrees with that of Mott insofar as the number of fragments is supposed to be proportional to radial particle velocity, its development is based upon an entirely different and empirical concept of "critical velocity of straining." Velocity of straining is defined as the rate of stretching of the surface of the shell and is equal to $(2\pi V)$. The critical velocity of straining corresponds to the minimum value of V for which fracture will occur. In the following, their basic formulation shall be employed.

At the outset, it is useful to point out the distinctive features of impulsive loads. Under static loads, stresses and strains are distributed throughout the body and local stress-concentrations are important. However, under impulsive loading transient stresses and strains may exist in highly localized regions, and the

fracture may not even propagate before another stress situation comes into play.

Impulsive loads set up stress waves in the medium. In the case of loading such as that occurring in the present case (blast wave hitting head-on into the shell), the waves generated are longitudinal. If the wave is one of compression, the particle velocity is in the same direction as the wave. And, if the wave is one of tension, the particle velocity is in the direction opposite to that of the wave. No information on formulae for wave propagation in thin spherical shells is available. The stress-wave propagation velocity may be anywhere between 3,000 - 21,000 feet/seconds (note that stress-wave propagation velocity is not the same as particle velocity). This should be compared to the fact that velocity of fracture is rarely more than 5,000 feet/seconds. M. Kolsky [30] has reported experiments on polystyrene plastic rods in which fracture starting along the axis did not extend to the surface. Apart from the fact of stress-concentration along the axis, this phenomenon may be attributed to the rapidly changing stress-situation, and hence, strain-rate. In any case, it is clear from the foregoing that it is not safe to assume fracture velocity as much

greater than velocity of straining under impulsive loading. This is especially true in the case of ductile materials where fracture velocity is extremely low.

3. On Shell Fragmentation

In order to study fracture of the shell it is first necessary to specify the loading. The shell is supposed to be loaded by detonating a chemical explosive at its geometric center. Ignition of the explosive at the geometric center of the shell will give rise to a spherical blast wave. Assuming that the shell has no effect on the detonation wave, the shock-wave collision with the shell will result in the latter's being loaded impulsively. The pressure rises instantaneously to its maximum value and then decays to zero in a very short time. It is thus clear that the loading here is not only dynamic but also impulsive.

The collision of the shock wave with the shell sets up a compression wave in the shell. This is illustrated in Figure 10a. When this wave reaches the outer surface it is reflected back as a tension wave and one has the situation shown in Figure 10b. The particle velocity is now obtained by superposition and is $2V$. Thus, after the shock wave strikes the shell surface, the shell is

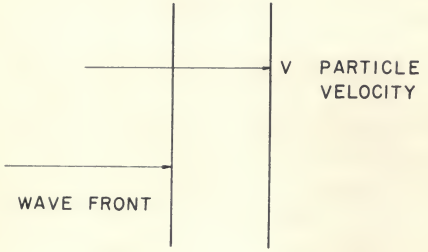

(a)

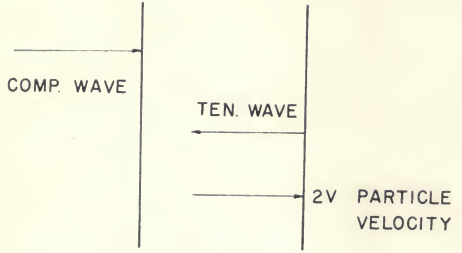

(b)

Figure 10: Propagation of Stress-Waves in Media

expanding at a very rapid rate. Following Rinehart and Pearson, a critical velocity of straining (V_{cr}) is postulated. Fracture will occur if the velocity of straining reaches the critical velocity of straining. If the spherical shell is radially expanding with a velocity V, then the rate of increase in surface area is given by $8 \pi R V$. The velocity of straining is now defined as equal to $8 \pi V$ and the critical velocity of straining as the one corresponding to the minimum value of V for which fracture will occur.

The question that must be answered now is whether the fracture will be of a shear (ductile) or tension (brittle) type. A tension fracture usually occurs during expansion of the shell. A shear fracture, on the other hand, will occur during release of compressive stress by the reflected tension stress wave. If fracture occurs during first compression wave, it will be of a brittle type. If, however, fracture does not occur during the first compression wave, it may turn out to be a complicated mixture of brittle and ductile types. This latter type has been observed in thick cylindrical shells [29]. The fracture behavior may also be further complicated by relatively high temperatures reached at the shock front [6] and consequent heating of the shell surface.

4. Experimental Program

In light of Rinehart and Pearson's expression for cylindrical shells, the following relationship is proposed for the number of fragments:

$$N = 8\pi \frac{V}{V_{cr}} \tag{40}$$

A logical experimental program is now to determine the ratio

$$N/V = \lambda^*$$

A number of experiments were conducted on polystyrene shells of several diameters. The shell-thickness was approximately 0.05 inches. Shells were loaded internally by detonating a PBRDX explosive. The combination used prior to assembly is reproduced in Figure 11. Two different sizes of charges were employed in the testing program i.e., (1) a spherical charge of 3/8 inch diameter varying in weight from 0.56 grams to 0.62 grams and (2) a spherical charge of 1/2 inch diameter varying in weight from 1.27 grams to 1.31 grams. These charges were mounted at the geometric center of the spheres when assembled from two matching hemispheres.

The experimental program was conducted in two parts. The first part consisted of experimental firings for high-

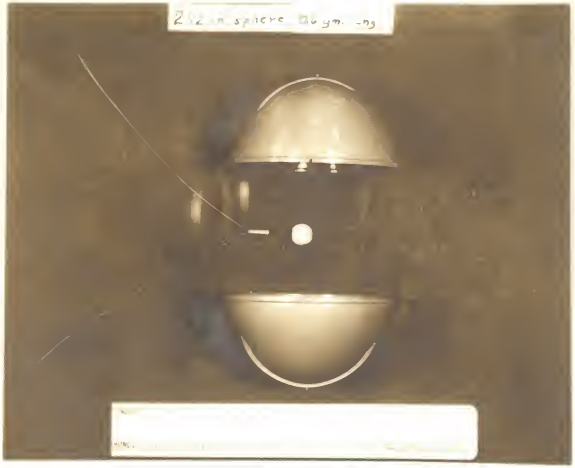

Figure 11: Combination of Shell, Detonator and Charge Prior to Assembly

speed measurements of case break-up. The second part consisted of similar experimental firings for recovery of fragments. It was not possible to obtain pictures and to recover fragments from the same experiment because of the need for an intense light source. The two sections are described below.

The photos were taken with a Beckman and Whitley framing camera, model 189 operating at 500,000 frames per second. The duration of the individual exposure was approximately 0.3 microseconds. Photo illumination was provided from a fourteen-inch cone filled with argon gas and initiated by a 100 gram charge of composition C-3. A typical photo-sequence is reproduced in Figure 12.

The recovery of fragments was never 100 per cent as the experimental firing bay is open on one side. However, it would appear that only a very small amount (less than 3-5 per cent) was lost as the weight of recovered fragments in the case when only the detonator was used equalled the weight prior to assembly. The discrepency between the weight before firing and the weight of the recovered fragments is because of the evaporation and burning of the plastic as a result of the intense heats reached at the shock-front hitting the shell. It is to

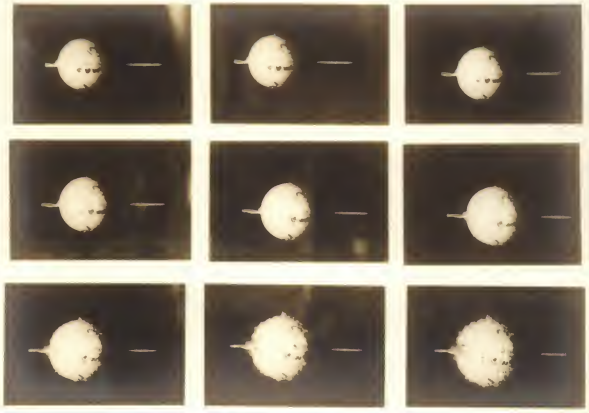

Figure 12: Fracture of 1 11/16 Inch Diameter Plastic Sphere. Charge Weight: 1.3 grams. Frame Rate: 500,000 Frames/Second

be observed that nearly one third of the plastic weight either evaporated or burned in each case. The fragments recovered were generally of three sizes i.e., (i) very large, (ii) moderate and (iii) extremely small bordering on fine powder. The number of fragments listed in Table 6 is nominal. It was found convenient to count the number of largest fragments equalling two thirds of the recovered weight and then multiply the number by 3/2. In justification of this process, it may be said that very small fragments may be neglected in first approximations. The value of particle velocity V was obtained directly from high-speed photographs. The last two columns in Table 6 represent calculated values.

The purpose of the experiments was two-fold i.e., (1) to study the nature of fracture and (2) to determine λ^*. The plastic spheres exhibited a great isotropy in fracture (see Figure 12) revealing a predominantly brittle fracture. The value of λ^* was calculated from observed values of V and N. It is seen from Table 6 that this value is the same within experimental limits, for the shell of a particular diameter regardless of the charge size. This is as it should be.

A result of still greater importance is the fact that $D^3 \lambda^*$ is a constant. Table 6 reveals that $D^3 \lambda^*$ varies

TABLE 6

EXPERIMENTAL RESULTS ON FRACTURE

Sphere diameter (D)	Charge size	Plastic mass before firing	Plastic mass after firing	No. of fragments (N)	V (ft/sec)	$\lambda^*=N/V$	$D^3 \lambda^*$
1 $\frac{5}{16}$ inch	0.6 gm	6.58 gm	4.65 gm	590	2700	0.219	0.495
	1.3 gm	6.58 gm	4.65 gm	680	2800	0.243	0.549
1 $\frac{11}{16}$ inch	0.6 gm	13.13 gm	8.75 gm	210	1980	0.106	0.509
	1.3 gm	13.25 gm	8.20 gm	260	2370	0.110	0.529
2 $\frac{1}{2}$ inch	0.6 gm	30.19 gm	19.80 gm	31	820	0.038	0.598
	1.3 gm	30.18 gm	19.30 gm	45	1200	0.038	0.598

by less than 10 per cent around a median value of 0.549. This agreement is extremely good in view of the various experimental limitations, such as, (1) difference in charge-sizes, (2) failure to center charges properly, (3) necessity of obtaining pictures and fragments from separate experiments, (4) failure to collect all fragments and (5) error in reading high-speed photographs. It goes without saying that elimination of one or several of these sources of error should yield substantially better agreement in the value of $D^3 \lambda^*$. It follows then from constancy of $D^3 \lambda^*$ that the critical velocity of straining (V_{cr}) is directly proportional to the cube of the shell diameter.

A part of the experimental program reported in Table 6 was repeated by filling the empty space between the charge and the plastic shell with water. The results are reproduced in Table 7. They show a remarkable agreement with the earlier results, confirming thereby once again the hypothesis that λ^* is independent of pressure for a particular shell-size. The present tests show a slightly higher value for $D^3 \lambda^*$. The difference is not, however, significant as the upper limit in the former case and the lower limit in the present case cross each other.

TABLE 7

ADDITIONAL EXPERIMENTAL RESULTS ON FRACTURE

Sphere diameter (D)	Charge size	Plastic mass before firing	Plastic mass after firing	No. of fragments (N)	V (ft/sec)	$\lambda^*=N/V$	$D^3 \lambda^*$
1 5/16 inch	0.6 gm	6.58 gm	5.0 gm	720	2750	0.262	0.592
	1.3 gm	6.58 gm	5.0 gm	960	3600	0.266	0.601
2 1/2 inch	0.6 gm	30.20 gm	20.7 gm	30	770	0.039	0.614
	1.3 gm	30.20 gm	22.7 gm	56	1350	0.041	0.645

5. Some Dimensional Considerations

In the preceding section, it was shown that V_{cr} is directly proportional to D^3. Now the effect of wall thickness (W_t) and material properties on V_{cr} shall be examined on the basis of dimensional analysis.

Since the shells under consideration are thin, shear effects may be neglected. The primary dimensional parameters are then (1) shell diameter (D), (2) wall thickness (W_t), (3) Young's modulus (E), and (4) density of material (ρ_m). The dependence of V_{cr} on these parameters may be expressed mathematically as

$$V_{cr} \propto D^3 f(W_t, E, \rho_m) \tag{41}$$

Assuming that it is possible to expand f in powers of W_t, E and ρ_m, (41) may be written as:

$$V_{cr} \propto D^3 \sum_i K_i W_{t_i}^{\nu'} E_i^{\nu''} \rho_{m_i}^{\nu'''} \tag{42}$$

where K_i, ν', ν'', ν''' are nondimensional constants and $i = 1, 2, 3, \cdots$

Then from dimensional analysis

$$\left[\frac{\bar{L}}{\bar{T}}\right] = \left[\bar{L}\right]^3 \left[\bar{L}\right]^{\nu'} \left[\frac{\bar{M}}{\bar{T}^2 \bar{L}}\right]^{\nu''} \left[\frac{\bar{M}}{\bar{L}^3}\right]^{\nu'''}$$

where $\bar{M}$, $\bar{L}$, $\bar{T}$ respectively denote dimensions of mass, length and time. Comparing exponents of $\bar{M}$, $\bar{L}$ and $\bar{T}$ on both sides, one finds

$$v' = -3$$
$$v'' = +1/2$$
$$v''' = -1/2$$

Therefore from equations (41) and (42) there follows

$$V_{cr} \propto \frac{D^3}{W_t^3} \sqrt{\frac{E}{\rho_m}} \tag{43}$$

It is now interesting to examine how the variables (D, W_t, E, ρ_m) effect the number of fragments. For a specified impulse, particle velocity V is inversely proportional to M^3 (M is mass of the shell) and hence to W_t^3. However, it is independent of material properties E and ρ_m. Then from (40), it becomes obvious that wall thickness has no effect on the number of fragments. Also, if one denotes by subscripts 1 and 2 two different materials, then

$$\frac{N_1}{N_2} \propto \sqrt{\frac{\rho_1 E_2}{\rho_2 E_1}} \tag{44}$$

Although the above results are derived from quite general considerations, it must be emphasized that they should be used with caution pending experimental confirmation as

several nondimensional parameters (such as Poisson's ratio) may also effect the behavior of shells.

6. Conclusions

Experimental tests on polystyrene shells confirm the possibility of extending the empirical criteria of Rinehart and Pearson for cylindrical shells to the case of spherical shells. Experimental results also prove that λ^* is dependent only upon shell-size and material and not upon the charge-size. Further, it was observed that V_{cr} is directly proportional to the cube of the shell-diameter. The fracture pattern was found to be isotropic and brittle. It is shown from dimensional analysis that wall thickness has no effect on the number of fragments. The effect of material properties is also investigated.

CHAPTER IV

ON THE CALCULATION OF FRACTURE-TIME FOR THIN SPHERICAL SHELLS SUBJECT TO INTERNAL BLAST LOADING

1. Introduction

In Chapter I, a similarity solution for obtaining the pressure behind the shock front in a spherically symmetric blast wave generated by a finite charge was outlined. This method was used in conjunction with experimental data to find the pressure distribution in the explosive gases behind the contact front in Chapter II. In Chapter III, the nature of fracture under impulsive loading was examined. An empirical formula for the number of fragments was proposed. It was shown that the number of fragments (N) was directly proportional to the particle velocity V (P) where P is the dynamic pressure. In the present Chapter, the relationship between V and P is examined through the introduction of the concept of fracture time. Fracture time is defined as the time which must elapse between the impact of the blast wave on the shell and the rupture of the shell. The general relation

between V and P is simplified by introduction of thin-shell assumptions. Finally, the relation is applied to the theoretical and experimental data previously reported in Chapters I - III.

2. Preliminary Considerations

The blast wave on hitting the shell imparts to it an impulse. This can be easily calculated by integrating $\left[p(t) + \rho(t)\, u^2(t)\right]$ from the time of impact (t=0) to the time of rupture (t_f) [31]. Mathematically:

$$I = 4\int_0^{t_f} \pi R^2 \left[p(t) + \rho(t) u^2(t)\right] dt \tag{45}$$

where R is the radius of the shell, p(t) the pressure acting on the surface of the shell, ρ(t) the density of the impinging gases and u(t) the velocity of the gases.

The impulse imported to the shell appears as the momentum (MV) of the shell. Thus

$$I = MV = 4\int_0^{t_f} \pi R^2 P\, dt \tag{46}$$

with

$$P = p + \rho u^2$$

M denotes the mass of the shell and V the particle velocity. Relation (46) is quite general. No assumptions have been introduced except for the fact that in proposing equation

(46) it is implicitly recognized that the energy dissipated in fracture is negligible in comparison to the total energy associated with the impulse. At this stage, certain assumptions are introduced in order to simplify equation (46). The first two are: (i) The blast wave is not affected by the shell i.e. reflection may be ignored. (ii) The dynamic pressure P remains constant during the fracture time t_f.

It is hard to justify these assumptions purely from theoretical reasoning. Later on, more will be said on this point. For the present, this shall be accepted as a working hypothesis.

So far, nothing was said about the shell thickness. In the following, under thin-shell assumptions, the structure of equation (46) will be examined.

3. Thin-Shell Simplifications

The impact of the blast wave on the shell-surface sets up longitudinal stress waves in the shell. The stress-wave propagation velocity may lie anywhere between 3,000 - 21,000 feet/second. Thus, the time for the head of the stress-wave to travel a distance of 0.05 inch (typical shell thickness employed in experiments reported in Chapter III) is of the order of (0.2 - 1.4) μsec. It

was observed that the fracture of the shell was primarily brittle and that it exhibited no scabbing. This implies that the fracture occurred during the onward first compression wave and before its reflection as a tension wave at the outer surface of the shell [29]. Hence, the fracture time (t_f) must lie in the range (0.2 - 1.4) μsec. For this order of time, no great decay occurs at the shock front (Chapter II). The decay is also balanced by reflection of the shock wave from the surface of the shell. It would seem reasonable, therefore, to take values of p as that existing just behind the shock front. The values of ρ and u are taken as those existing across the contact front as gases in the contact front have a much higher density than compressed air. Then equation (46) becomes

$$M V = 4\pi R^2 \bar{P} t_f$$

and, hence,

$$t_f = \frac{MV}{4\pi R^2 \bar{P}} \qquad (47)$$

4. Experimental Results

Experimental results, involving the measurement and calculation of the pressure at the shock front resulting from exploding PBRDX charges, were reported in Chapter II.

The first six columns in Table 8 are based upon these results.* Columns 7 and 8 are reproduced from Chapter III* (Table 6), where the behavior of a plastic shell under blast loading (charges employed were identical with those in Chapter II) is discussed. The last column reports fracture time calculated by employing equation (47).

It is seen that the fracture time t_f is consistently less for the larger charge indicating that the fracture time is dependent upon dynamic pressure P. This is to be expected as the impulse I imparted to the shell and the particle velocity V depend upon the dynamic pressure P.

The fracture time is of the order of (0.6-2.0) μsec. This is approximately twice what one would expect from theoretical analysis of stress wave propagation. The discrepancy is due to the neglect of reflection. If even a simple reflection law is accepted, it would double the dynamic pressure (P) and thus reduce the fracture time by half.

---

*In Table 8, all the units employed belong to the CGS system regardless of units used in Chapters II and III.

TABLE 8

CALCULATION OF FRACTURE TIMES

Charge Size (gms)	Sphere Radius (R) cms	Pressure (p) dynes/cm^2 10^6	Density (ρ) gm/cm^3 10^{-3}	Velocity of gases (u) cm/sec 10^3	Dynamic Pressure (P) dynes/cm^2 10^8	Mass of sphere (M) gms	Particle Velocity of sphere (V) cm/sec 10^4	Fracture Time (t_f) μsec
0.6	1.667	293	79	502	202.1	6.58	8.230	0.77
	2.143	194	57	409	97.3	13.13	6.035	1.41
	3.175	99	34	292	30.0	30.19	2.499	1.99
1.3	1.667	321	92	537	268.5	6.58	8.534	0.60
	2.143	229	71	454	148.6	13.25	7.224	1.12
	3.175	133	47	346	57.6	30.18	3.658	1.51

CHAPTER V

CONCLUSIONS

On the basis of preceding mathematical and empirical analysis, following conclusions may be drawn:

(1) There exists a group of similarity transformations for the case of axisymmetric flow when the Euler equations are given in spherical coordinates. It is possible to employ this set of transformations along with empirical data to obtain approximate solutions for the spherically symmetric and axisymmetric blast waves generated by point-source or finite-source explosions.

(2) Dominant fracture pattern in thin polystyrene spherical shells under internal blast loading is brittle. The number of fragments (N) is inversely proportional to the critical velocity of straining (V_{cr}). It is, however, independent of the wall thickness of the shell. Also, critical velocity of straining (V_{cr}) is directly proportional to the shell-diameter (D).

(3) The fracture-time (t_f) depends upon dynamic pressure (P) and decreases with increasing P.

LIST OF REFERENCES

1. Jones, H., and Miller, A. R., "The Detonation of Solid Explosives: the Equilibrium Conditions in the Detonation Wave-Front and the Adiabatic Expansion of the Products of Detonation," Proceedings Royal Society (London), A, Vol. 194, p. 480, (1948).

2. Zeldovich, Ia. B., and Kompaneets, A. S., Theory of Detonation, Academic Press, New York, Chapter 5, (1960).

3. Taylor, G. I., "The Dynamics of the Combustion Products behind Plane and Spherical Detonation Fronts in Explosives," Proceedings Royal Society (London), A, Vol. 200, p. 235, (1950).

4. Oppenheim, A., et al., "Recent Progress in Detonation Research," AIAA Journal, (Oct., 1963).

5. Glass, I. I., "Aerodynamics of Blasts," UTIAS Review No. 17, (1960).

6. Taylor, G. I., "The Formation of a Blast Wave by a Very Intense Explosion," Proceedings Royal Society (London), A, Vol. 201, p. 159, (1950).

7. Sedov, L. I., Similarity and Dimensional Methods in Mechanics, Academic Press, New York, (1959).

8. von Neumann, J., Collected Works, Vol. VI, The Macmillan Company, New York, (1963).

9. Taylor, J. L., Philosophical Magazine, Vol. 46, p. 317, (1955).

10. Latter, R., "Similarity Solution for Spherical Shock Wave," Journal of Applied Physics, Vol. 26, No. 8, p. 954, (1955).

LIST OF REFERENCES (Continued)

11. McFadden, J. A., "Initial Behavior of a Spherical Blast," Journal of Applied Physics, Vol. 23, No. 11, (1952).

12. Brode, H. L., "Blast Wave from a Spherical Charge," Physics of Fluids, Vol. 2, p. 217, (1959).

13. Berry, F. J., et al., "Early Development of Spherical Blast from Particular Charge," Proceedings Royal Society (London), A, Vol. 227, p. 258, (1955).

14. Taylor, G. I., "The Air Wave Surrounding an Expanding Sphere," Proceedings Royal Society (London), A, Vol. 200, p. 235, (1946).

15. Bradley, J. N., Shock Waves in Chemistry and Physics, John Wiley and Sons, Inc., New York, Chapter III, (1962).

16. Morgenroth, H., "Zur Frage der nichtstationären ebenen stosswellen mit Zeitlich Veränderlicher Gesamtenergie," Annalen der Physik, 7 Folge, Band 9, Heft 3-4, p. 212, (1962).

17. Rogers, M. H., Quarterly Journal of Mechanics and Applied Mathematics, Vol. XI, p. 411, (1958).

18. Wecken, F., Mem. 14m. Lab Recherches Tech. Saint-Louis, (1951).

19. Buckingham, R. A., Numerical Methods, Sir Isaac Pitman and Sons, Ltd., London, p. 241, (1962).

20. Jones, D. L., "Strong Blast Waves in Spherical, Cylindrical and Plane Shocks," Physics of Fluids, Vol. 4, p. 1183, (1961).

21. Cranz, C., and Schardin, H., "Kinematographie auf ruhendem Film und mit extrem hoher Bildfrequenz," Zeits. für Physik, Vol. 56, p. 147, (1930).

22. North, R. J., "A Cranz-Schardin High-Speed Camera for Use with a Hypersonic Shock Tube," NPL/Aero/399, (1960).

LIST OF REFERENCES (Continued)

23. DeLeeuw, J. H., et al., "A High-Speed Multi-Source Spark Camera," UTIAS Tech. Note, No. 26, (1962).

24. Schardin, H., "Measurement of Spherical Shock Waves," Communications on Pure and Applied Mathematics, Vol. 7, p. 223, (1954).

25. Griffith, A. A., "The Phenomena of Rupture and Flow in Solids," Transactions Royal Society (London), A, Vol. 221, p. 163, (1921).

26. Orowan, E., "Fundamentals of Brittle Behavior in Metals," Contribution to a Conference on Fatigue and Fracture of Metals at MIT, (1950).

27. Irwin, G., "Fracture Dynamics," Fracturing of Metals, A.S.M., p. 147, (1948).

28. Mott, N. F., "Fragmentation of Shell Cases," Proceedings Royal Society (London), A, Vol. 189, p. 300, (1946).

29. Rinehart, J. S., and Pearson, J., Behavior of Metals under Impulsive Loading, A.S.M., p. 123. (1954).

30. Kolsky, M., "Fractures Produced by Stress Waves," Fracture (Proceedings of a Conference on Fracture at MIT), John Wiley and Sons, New York, p. 281, (1959).

31. Ruedenberg, R., "Über die Fortpflanzungsgeschwindigkeit und Impulsstaerke von Verdichtungsstoessen, Artillerist. Monatshefte, No. 113, p. 237, (May, 1916), [Quoted in Doering, W. and Burkhardt, G., "Contributions to the Theory of Detonation," Translated from German at Brown University, Tech. Rpt. No. F-TS-1227-1A (GDAM A9-T-46), p. 101, (May, 1949)].

BIOGRAPHICAL SKETCH

Sabodh K. Garg was born at Bhatinda in northwest India. He was graduated in July, 1960, from Panjab University (India) with the degree of Bachelor of Arts, Honours (English Literature, Mathematics); and in August, 1962, from the University of Florida with the degree of Master of Science in Engineering (Engineering Mechanics, Mathematics). During the summer months of 1963 and 1964, he attended University of Oslo International Summer School (Norway) and Plasma Physics Institute at Princeton University, respectively.

This dissertation was prepared under the direction of the chairman of the candidate's supervisory committee and has been approved by all members of that committee. It was submitted to the Dean of the College of Engineering and to the Graduate Council, and was approved as partial fulfillment of the requirements for the degree of Doctor of Philosophy.

June, 1965

Thomas L. Martin Jr.
Dean, College of Engineering

Dean, Graduate School

Supervisory Committee:

I. Lieberman
Chairman
William A. Nash
Harling K. Flesch
R. J. Blake